Article

Lorentz Forces Effects on the Interactions of Nanoparticles in Emerging Mechanisms with Innovative Approach

Noor Saeed Khan [1,2,3,*] , **Qayyum Shah** [4,5], **Arif Sohail** [6], **Poom Kumam** [1,2,7,*] , **Phatiphat Thounthong** [8] , **Amiya Bhaumik** [5] and **Zafar Ullah** [3]

1   KMUTTFixed Point Research Laboratory, Room SCL 802 Fixed Point Laboratory, Science Laboratory Building, Department of Mathematics, Faculty of Science, King Mongkut's University of Technology Thonburi (KMUTT), Bangkok 10140, Thailand

2   Center of Excellence in Theoretical and Computational Science (TaCS-CoE), Science Laboratory Building, Faculty of Science, King Mongkut's University of Technology Thonburi (KMUTT), 126 Pracha-Uthit Road, Bang Mod, Thrung Khru, Bangkok 10140, Thailand

3   Division of Science and Technology, Department of Mathematics, University of Education, Lahore 54000, Pakistan; zafar.ullah@ue.edu.com

4   Department of Basic Sciences and Islamiyat, University of Engineering & Technology, Peshawar, Khyber Pakhtunkhwa 25000, Pakistan; qayyumshah@uetpeshawar.edu.pk

5   Faculty of Engineering, Lincoln University College (LUC), Kelantan 15050, Malaysia; amiya@lincoln.edu.my

6   Department of Mathematics, Islamia College University, Peshawar, Khyber Pakhtunkhwa 25000, Pakistan; arif.sohail.khattak@gmail.com

7   Department of Medical Research, China Medical University Hospital, China Medical University, Taichung 40402, Taiwan

8   Renewable Energy Research Centre, Department of Teacher Training in Electrical Engineering, Faculty of Technical Education, King Mongkut's University of Technology North Bangkok, 1518 Pracharat 1 Road, Wongsawang, Bangsue, Bangkok 10800, Thailand; phatiphat.t@ieee.org

*   Correspondences: noorsaeedkhankhattak@gmail.com (N.S.K.); poom.kum@kmutt.ac.th (P.K.)

check for updates

Abstract: This paper focuses on advances in the understanding of both the fundamental and applied aspects of nanomaterials. Nanoparticles (titania and graphene oxide) in water-based fluid lying on a surface incorporating the leading edge accretion (or ablation) are analyzed. Entropy generation rate is also considered. The Hall current effect is induced in the flow of hybrid nanofluid, due to which the two-dimensional study converts into three-dimensional space. Similarity transformations convert the equations of momentum, heat transfer, nanoparticles volume fraction and boundary conditions into non-dimensional form. Mathematica software is used to obtain the computation through homotopy analysis method. Analysis is provided through the effects of different parameters on different profiles by sketching the graphs. Flow, heat transfer and nanoparticles concentration in TiO_2/H_2O, as well as GO-TiO_2/H_2O, are decreased with increasing the Stefan blowing effect, while entropy generation rate elevates upon increasing each parameter. Both of the velocity components are reduced with increasing the Hall parameter. Streamlines demonstrate that trapping is increased at the left side of the surface. The obtained results are compared with the published work which show the authentication of the present work.

Keywords: hybrid nanofluid; nanoparticles; Hall current effect; leading edge accretion or ablation; entropy generation rate; homotopy analysis method

1. Introduction

When an electrically conducting fluid is under an ionization process and the strength of the applied magnetic field is high, then the normal conductivity of the magnetic field is reduced to the free spiraling of electrons and ions about the magnetic lines force before suffering collisions. In such a situation, a current is induced in a normal direction to both the electric and magnetic fields. This phenomenon is known as the Hall current effect. When the strength of the magnetic field is strong, the effects of Hall currents cannot be neglected. It is highly important and interesting to know how the results of hydrodynamical problems get modified by the effects of Hall currents. The Hall effect generates a cross flow, making the flow three-dimensional in a two-dimensional system. The magnetohydrodynamic flows with Hall effect have important applications in Hall accelerators, power generators, flight magnetohydrodynamics, refrigeration coils, transmission lines, electric transformers. Shateyi and Motsa [1] analyzed the problem of magnetohydrodynamic flow and heat transfer of a viscous, incompressible and electrically conducting fluid past a semi-infinite unsteady stretching sheet. Hayat et al. [2] investigated the viscous dissipation effects on mixed convection three-dimensional flow of Jeffery fluid past a vertical stretching surface taking into account the Hall and ion effects. Ahmed and Zueco [3] obtained the exact solution to the problem of heat and mass transfer in a rotating vertical porous channel in the presence of Hall current. Gaffar et al. [4] presented the nonlinear, non-isothermal, magnetohydrodynamic free convection boundary layer flow, heat and mass transfer of non-Newtonian Eyring–Powell fluid from a vertical surface in a non-Darcy, isotropic, homogeneous porous medium considering Hall currents and ionslip currents. Abdelaziz [5] worked on the steady boundary layer magnetohydrodynamic slip flow past a stretching sheet in a water-based nanofluid in the presence of the Hall effect. Hayat et al. [6] investigated the Hall effect on the peristaltic transport of couple stress fluid in an inclined channel.

Structure and dynamics, particularly surfaces and interfaces, have long been fields of fruitful research. This field has changed profoundly since the discovery of nanoparticles. While nanoparticles continue to dazzle the research community with recent discoveries such as superconductivity and highly correlated electron physics, a plethora of other materials have emerged, covering an entire spectrum of electronic properties. Moreover, the possibility of stacking these materials to create artificial structures, interfaces, and with tunable twisting angles, opens the door to unprecedented control of structure, dynamics, and properties. We now possess exquisite control in designing new model systems, exploring new properties, and studying new physical/chemical processes. Recently, the focus has been on advances in the understanding of both the fundamental and applied aspects of nanoparticles and nanofluids for researchers and practicing engineers from different disciplines to interact and exchange their latest understandings. Khan [7] analyzed the nanobioconvection model to explore that Brownian motion parameter increases the thermal conductivity and creates resistance to the flow of microorganisms. Bahiraei and Heshmation [8] presented a review examining the graphene family nanofluids for the capabilities of graphene-based nanofluids, innovations in preparing techniques, stability analysis and types of surfactants used. They provided future work and also investigated the second law analysis for graphene-family nanofluids, thermophysical properties, hydrodynamic attributes, boiling and convective heat transfer, as well as the applications such as in car radiators, electronic coolings, heat exchangers, energy storage, in addition to molecular dynamics and artificial intelligence. Briffa et al. [9] worked on the physical and chemical transformations of zirconium-doped ceria nanoparticles in the presence of phosphate. Khan et al. [10] used rheological equations of an isotropic Casson nanofluid and Williamson nanofluid to asses the flow, heat transfer, nanoparticles concentration and gyrotactic microorganisms. Bahiraei [11] attempted to work on the past studies related to nanofluids in review and summary form, considering particle migration, Buongiorno model, molecular dynamics simulation, and other theoretical studies. He concluded about the research related to nanofluids (mentioned in his paper) that among

other reasons, particle migration is the reason which causes inconsistencies in the previous studies results. Saba et al. [12] studied hybrid nanofluid (CNT-Fe_3O_4/H_2O) in asymmetric long channel with dilating/squeezing walls by implementing the active method coupled with the RK–Fehlberg algorithm for the solution of non-dimensional equations. Bahiraei et al. [13] reviewed and summarized the present investigations for nanofluids in heat exchangers. They found that excessive reports have proven that nanofluids provide an enhanced heat transfer rate which increases by incrementing the concentration and Reynolds number. Waini et al. [14] investigated dual solutions and temporal stability analysis of the dual solutions for the unsteady flow and heat transfer in a hybrid nanoflid past a stretching/shrinking sheet. Bahiraei and Heshmation et al. [15] reviewed the use of nanofluids in electronics cooling by considering several aspects like block type, nanoparticle material, numerical approach, energy consumption and second law of thermodynamical system to show the challenges offered in the field under study. Gulzar et al. [16] presented an experimental study on the rheological behaviour and stability analysis of Al_2O_3-TiO_2 Therminol-55 hybrid nanofluid using varying concentrations of 0.05 wt%, 0.075 wt%, 0.1 wt%, 0.25 wt% and 0.5 wt% in two-step method. Dalkilic et al. [17] worked experimentally on the turbulent heat transfer characteristics of Graphite-SiO_2/H_2O hybrid nanofluid flow in a horizontal smooth tube with and without quad-channel twisted tape inserts of length between 0 and 42 cm with constant ratios of 5. Khan et al. [18] discussed the effective thermal conductivity, particle's conventional static and a Brownian motion which describes the influences of size, volume fraction, temperature dependency, the type of particle and base fluid combination. Rosca et al. [19] used Buongiorno's nanofluid model to investigate the unsteady boundary layer flow of a nanofluid past a moving surface in an external uniform free stream. More studies on fluids and analytical solutions are presented in the references [20–37].

Entropy generation reduces the performance of engineering systems due to irreversibilities which exists in heat and mass transfer flows. The first attention to the entropy generation was paid by Bejan [38]. Ahmad and Nadeem [39] used the Thomson and Troian auxiliary conditions to investigate the entropy minimization in stagnation point flow of a hybrid nanofluid with Cattaneo–Christov heat and mass flux theory, variable mass diffusivity and viscosity, activation energy past a nonlinear porous stretching sheet. Khan et al. [40] applied the shooting method to compute the solution of entropy generation in axisymmetric flow of non-Newtonian nanofluid between two parallel rotating disks where Bejan number was noted to decrease with increasing the parameter of Casson nanofluid. Khan et al. [41] examined the entropy generation for single/multi walled carbon nanotubes with homogeneous–heterogeneous chemical reactions and heat transfer. Zaib et al. [42] proposed a mathematical model for entropy generation considering micropolar magnetite-Fe_3O_4 ferro liquid to compute the first and second solutions of the problem. Khan et al. [43] worked for the first time in the literature to measure the entropy generation in the presence of gyrotatic microorganisms whose investigations showed that entropy generation was increased with the microorganisms concentration difference parameter. Shahsavar et al. [44] applied the two-phase mixture model to simulate the hydrothermal and irreversibility behavior of biological water–Ag nanofluid by finding that with decreasing the average nanofluid temperature, thermal conductivity was decreased, which resulted in the decrement of entropy generation. Khan et al. [45] used the series solution to analyze the entropy generation in the presence of the Hall effect, buoyancy effects, thermal radiation, Soret and Dofour effects. Sohail et al. [46] communicated through the entropy generation of three-dimensional flow of Maxwell nanofluid containing gyrotactic microorganisms and homogeneous–heterogeneous chemical reactions in the presence of Cattaneo–Christov heat and mass flux theory, which showed that entropy generation increased with high values of thermal radiation. Shah et al. [47] reported the entropy generation in non-Newtonian Casson nanofluid flow with thermal radiation, Arrhenius activation energy and binary chemically reaction past a nonlinear stretching surface. Khan et al. [48] investigated hybrid nanofluid flow with entropy generation. The references [49–52] provide a few other studies on the entropy subject.

The aforementioned discussion rests on the analysis of different features of fluids, but still there is a gap in the discussion of hybrid nanofluids with Hall effect and entropy generation in the literature. The objective of the present study is to investigate further the hybrid nanofluid. Hence, the authors have attempted to model and solve the problem for hybrid nanofluid with leading edge accretion or ablation, Hall effect and entropy generation, whose solution is accomplished through HAM [53].

2. Methods

An incompressible viscous fluid flow is investigated with free stream velocity U_∞, nanoparticles concentration C and temperature T. In water-based fluid, two types of nanoparticles, namely TiO$_2$ (titania) and GO (graphene oxide), with volume fractions $\phi_1 = 0.03$ and $\phi_2 = 0.04$ are considered respectively. Magnetic field $B = [0, B_0, 0]$ is applied perpendicularly to the heat and mass transfer flow. It is assumed that the strength of electric charge and magnetic field are maximum. The schematic diagram of the problem is shown in Figure 1.
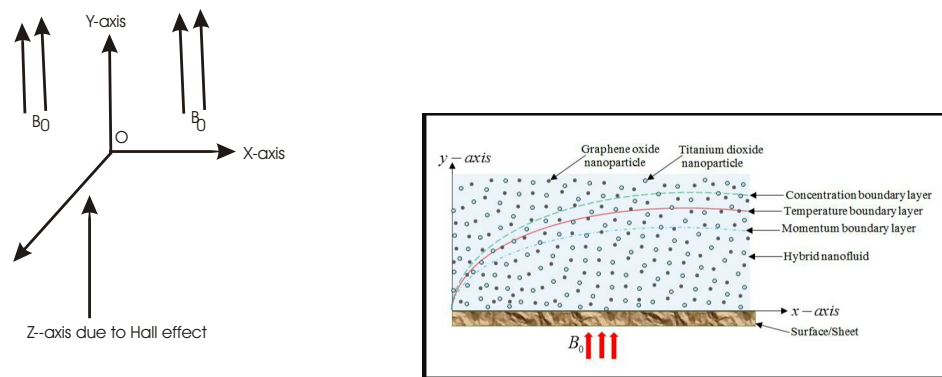

Figure 1. Schematic diagram of the problem.

The problem has the following governing equations for hybrid nanofluid as in [19,45]

$$\frac{\partial u}{\partial x} + \frac{\partial v}{\partial y} + \frac{\partial w}{\partial z} = 0, \tag{1}$$

$$\frac{\partial u}{\partial t} + u\frac{\partial u}{\partial x} + v\frac{\partial u}{\partial y} = U_\infty\frac{\partial U_\infty}{\partial x} + \frac{\mu_{hnf}}{\rho_{hnf}}\frac{\partial^2 u}{\partial y^2} - \frac{\sigma_{hnf}B_0^2(u+mw)}{\rho_{hnf}(1+m^2)}, \tag{2}$$

$$\frac{\partial w}{\partial t} + u\frac{\partial w}{\partial x} + v\frac{\partial w}{\partial y} = U_\infty\frac{\partial U_\infty}{\partial x} + \frac{\mu_{hnf}}{\rho_{hnf}}\frac{\partial^2 w}{\partial y^2} + \frac{\sigma_{hnf}B_0^2(mu-w)}{\rho_{hnf}(1+m^2)}, \tag{3}$$

$$\frac{\partial T}{\partial t} + u\frac{\partial T}{\partial x} + v\frac{\partial T}{\partial y} = \frac{k_{hnf}}{(\rho c_P)_{hnf}}\frac{\partial^2 T}{\partial y^2} + \frac{\mu_{hnf}}{(\rho c_P)_{hnf}}\left[\frac{\partial u}{\partial y}\right]^2, \tag{4}$$

$$\frac{\partial C}{\partial t} + u\frac{\partial C}{\partial x} + v\frac{\partial C}{\partial y} = D_m\frac{\partial^2 C}{\partial y^2}, \tag{5}$$

where u, v, w are the velocity components in the x, y, z directions and m is the Hall parameter. The subscript hnf denotes the hybrid nanofluid. μ_{hnf}, ρ_{hnf}, k_{hnf} and $(\rho c_P)_{hnf}$ are respectively the dynamic viscosity, density, thermal conductivity and heat capacity of hybrid nanofluid.

Boundary conditions are used as

$$u = u_w = \lambda U_\infty, \quad v = -\frac{D_m}{1 - C_w}\frac{\partial C}{\partial y}, \quad w = 0, \quad T = T_w, \quad C = C_w, \quad at \quad y = 0, \tag{6}$$

$$u = u_e = U_\infty, \quad w \to 0, \quad T \to T_\infty, \; C \to C_\infty, \quad as \quad y \to \infty, \tag{7}$$

where u_e is the external velocity and λ is the stretching/shrinking parameter. $\lambda > 0$ is used for stretching sheet, $\lambda < 0$ is used for shrinking sheet and $\lambda = 0$ denotes the static surface. (T_w, C_w) and (T_∞, C_∞) are the hybrid nanofluid temperature and volume fractions at surface and infinity respectively. The thermophysical properties of water, titania and graphene oxide nanoparticles are given in Table 1, while the mathematical forms of the thermophysical properties of nanofluid and hybrid nanofluid are given in Table 2.

Table 1. Thermophysical properties of water and nanoparticles [12,14,39].

Thermophysical Properties	H₂O	TiO₂ (Titania)	GO (Graphene Oxide)
ρ (Density) (kg/m^3)	$\rho_f = 997.1$	$\rho_{s_1} = 4250$	$\rho_{s_2} = 1800$
c_P (Heat capacity) (J/kg K)	$(c_P)_f = 4179$	$(c_P)_{s_1} = 686.2$	$(c_P)_{s_2} = 717$
k (Thermal conductivity) (W/m K)	$k_f = 0.613$	$k_{s_1} = 8.9538$	$k_{s_2} = 5000$
σ (Electrical conductivity) (Um)$^{-1}$	$\sigma_f = 0.05$	$\sigma_{s_1} = 2.38 \times 10^6$	$\sigma_{s_2} = 1.1 \times 10^{-5}$

In Table 1, s$_1$ and s$_2$ are used respectively for the solid nanoparticles of TiO$_2$ (titania) and GO (graphene oxide). f is used for the base fluid.

Table 2. Formulations of thermophysical properties of nanofluid and hybrid nanofluid [12,14,39].

Properties	Nanofluid (TiO₂/H₂O)
Density (ρ)	$\rho_{nf} = (1 - \phi)\rho_f + \phi\rho_s$
Heat capacity (ρc_P)	$(\rho c_P)_{nf} = (1 - \phi)(\rho c_P)_f + \phi(\rho c_P)_s$
Dynamic viscosity (μ)	$\frac{\mu_{nf}}{\mu_f} = \frac{1}{(1-\phi)^{2.5}}$
Thermal conductivity (k)	$\frac{k_{nf}}{k_f} = \frac{k_s + 2k_f - 2\phi(k_f - k_s)}{k_s + 2k_f + \phi(k_f - k_s)}$
Electrical conductivity (σ)	$\frac{\sigma_{nf}}{\sigma_f} = 1 + \frac{3(\sigma - 1)\phi}{(\sigma + 2) - (\sigma - 1)\phi}$, where $\sigma = \frac{\sigma_s}{\sigma_f}$
Properties	Hybrid nanofluid (GO-TiO₂/H₂O)
Density (ρ_{hnf})	$\rho_{hnf} = (1 - (\phi_1 + \phi_2))\rho_f + \phi_1\rho_{s_1} + \phi_2\rho_{s_2}$
Heat capacity $(\rho c_P)_{hnf}$	$(\rho c_P)_{hnf} = (1 - (\phi_1 + \phi_2))(\rho c_P)_f + \phi_1(\rho c_P)_{s_1} + \phi_2(\rho c_P)_{s_2}$
Dynamic viscosity (μ_{hnf})	$\frac{\mu_{hnf}}{\mu_f} = \frac{1}{\left[1 - (\phi_1 + \phi_2)\right]^{2.5}}$
Thermal conductivity (k_{hnf})	$\frac{k_{hnf}}{k_f} = \frac{\phi_1 k_{s_1} + \phi_2 k_{s_2} + 2\phi k_f + 2(\phi_1 k_{s_1} + \phi_2 k_{s_2}) - 2\phi^2 k_f}{\phi_1 k_{s_1} + \phi_2 k_{s_2} + 2\phi k_f - (\phi_1 k_{s_1} + \phi_2 k_{s_2}) + \phi^2 k_f}$
Electrical conductivity (σ_{hnf})	$\frac{\sigma_{hnf}}{\sigma_f} = 1 + \frac{3\left[\frac{\sigma_1\phi_1 + \sigma_2\phi_2}{\sigma_f} - (\phi_1 + \phi_2)\right]}{2 + (\frac{\sigma_1\phi_1 + \sigma_2\phi_2}{(\phi_1 + \phi_2)\sigma_f}) - \left[\frac{\sigma_1\phi_1 + \sigma_2\phi_2}{\sigma_f} - (\phi_1 + \phi_2)\right]}$

Introducing the similarity transformations for (f, g), ζ, θ, and φ as the non-dimensional velocities, variable, temperature and nanoparticles concentration respectively as

$$\psi(x, y, t) = U_\infty\sqrt{\nu_f t \cos\gamma + (\nu_f x/U_\infty)\sin\gamma}f(\zeta), \quad w = U_\infty\sqrt{\nu_f t \cos\gamma + (\nu_f x/U_\infty)\sin\gamma}g(\zeta)$$

$$u = \frac{\partial\psi}{\partial y}, \quad v = -\frac{\partial\psi}{\partial x}, \quad \zeta = y/\sqrt{\nu_f t \cos\gamma + (\nu_f x/U_\infty)\sin\gamma}, \quad \theta(\zeta) = \frac{T - T_\infty}{T_w - T_\infty} =, \quad \varphi(\zeta) = \frac{C - C_\infty}{C_w - C_\infty}, \tag{8}$$

where ψ is the stream function. ν_f is the kinematic viscosity. γ is the leading edge accretion or ablation parameter where $(\nu_f t \cos\gamma + (\nu_f x/U_\infty)\sin\gamma)$ must be greater than zero [19].

The continuity Equation (1) is identically satisfied through Equation (8). Information is deducted from Tables 1 and 2 and Equation (8) to get the following equations from Equations (2)–(7)

$$\frac{1}{\Phi_1 \Phi_2} f''' + \frac{1}{2}(\cos\gamma)\zeta f'' + \frac{1}{2}(\sin\gamma)ff'' - \Phi_5 \frac{M(f'+mg)}{1+m^2} = 0, \tag{9}$$

$$\frac{1}{\Phi_1 \Phi_2} g'' + \frac{1}{2}(\sin\gamma)fg' + \frac{1}{2}(\cos\gamma)\zeta g'' + \Phi_5 \frac{M(mf'-g)}{1+m^2} = 0, \tag{10}$$

$$\frac{1}{Pr}\frac{\Phi_4}{\Phi_3}\theta'' + \frac{1}{2}\left[(\sin\gamma)f + (\cos\gamma)\zeta\right]\theta' + \frac{1}{\Phi_1 \Phi_3}Ec f''^2 = 0, \tag{11}$$

$$\varphi'' + \frac{1}{2}Sc\left[(\sin\gamma)f + \zeta(\cos\gamma)\right]\varphi' = 0, \tag{12}$$

$$f = \frac{2}{Sc}\frac{1}{\sin\gamma}f_w\varphi', \quad f' = \lambda, \quad g = 0, \quad \theta = 1, \quad \varphi = 1, \quad at \quad \zeta = 0, \tag{13}$$

$$f' = 1, \quad g = 0, \quad \theta = 0, \quad \varphi = 0, \quad at \quad \zeta = \infty, \tag{14}$$

where $\Phi_1 = \left[1-(\phi_1+\phi_2)\right]^{2.5}$, $\Phi_2 = \phi_1\frac{\rho_{s_1}}{\rho_f} + \phi_2\frac{\rho_{s_2}}{\rho_f} + (1-(\phi_1+\phi_2))$, $\Phi_3 = \phi_1\frac{(\rho c_P)_{s_1}}{(\rho c_P)_f} + \phi_2\frac{(\rho c_P)_{s_2}}{(\rho c_P)_f} + (1-(\phi_1+\phi_2))$, $\Phi_4 = \frac{\phi_1 k_{s_1} + \phi_2 k_{s_2} + 2\phi k_f + 2\phi(\phi_1 k_{s_1} + \phi_2 k_{s_2}) - 2\phi^2 k_f}{\phi_1 k_{s_1} + \phi_2 k_{s_2} + 2\phi k_f - \phi(\phi_1 k_{s_1} + \phi_2 k_{s_2}) + \phi^2 k_f}$,

$\Phi_5 = 1 + \dfrac{3\left[\frac{\sigma_1\phi_1+\sigma_2\phi_2}{\sigma_f} - (\phi_1+\phi_2)\right]}{2+\left[\frac{\sigma_1\phi_1+\sigma_2\phi_2}{(\phi_1+\phi_2)\sigma_f}\right] - \left[\frac{\sigma_1\phi_1+\sigma_2\phi_2}{\sigma_f} - (\phi_1+\phi_2)\right]}$. (′) represents the derivative with respect to ζ.

$M = \dfrac{B_0^2}{\sqrt{\nu_{hnf}t\cos\gamma + (\nu_{hnf}x/U_\infty)\sin\gamma}}$ is the magnetic field parameter, $Pr = \dfrac{\mu_f(c_P)_f}{k_f}$ is the Prandtl number, $Ec = \dfrac{(U_\infty)^2}{(c_P)_f(T_w-T_\infty)}$ is the Eckert number, $Sc = \dfrac{\mu_f}{\rho_f D_m}$ is the Schmidt number, and $f_w = \dfrac{C_w-C_\infty}{1-C_\infty}$ is the suction/injection parameter (or Stefan blowing) respectively. It is noted that for $\phi_1 = 0.00$ and $\phi_2 = 0.00$, the problem becomes about viscous fluid. If $\phi_1 = 0.00$, GO/H_2O is obtained and if $\phi_2 = 0.00$, TiO_2/H_2O is made.

It is important to investigate the physical quantities having extensive applications in industries like the local skin friction coefficients (C_{f_x}, C_{g_z}), Nusselt number Nu_x, and wall mass flux Q_{mx} as

$$C_{f_x} = \frac{\tau_{w_x}}{\rho_{hnf}U_\infty^2}, \quad C_{g_z} = \frac{\tau_{w_z}}{\rho U_\infty^2}, \quad Nu = \frac{q_w x}{k_{hnf}(T_w-T_\infty)}, \quad Q_{mx} = \frac{q_m x}{D_B(C_w-C_\infty)}, \tag{15}$$

where

$$\tau_{w_x} = \left[\mu_{hnf}\frac{\partial u}{\partial y}\right]_{y=0}, \quad \tau_{w_z} = \left[\mu_{hnf}\frac{\partial w}{\partial y}\right]_{y=0}, \quad q_w = -k_{hnf}\left[\frac{\partial T}{\partial y}\right]_{y=0}, \quad q_m = -D_B\left[\frac{\partial C}{\partial y}\right]_{y=0}. \tag{16}$$

Note that (τ_{w_x}, τ_{w_z}), q_w, and q_m are known as wall frictions, heat transfer, and mass transfer on the surface respectively.

Utilizing Equation (16) in Equation (15) with Equation (8), it proceeds to

$$C_{f_x} = (Re_x)^{\frac{-1}{2}} \frac{1}{\Phi_1} f''(0) \frac{1}{\sqrt{\sin \gamma + \cos \gamma \sigma_1}}, \quad C_{g_z} = (Re_x)^{\frac{-1}{2}} \frac{1}{\Phi_1} g'(0) \frac{1}{\sqrt{\sin \gamma + \cos \gamma \sigma_1}},$$

$$Nu_x = -(Re_x)^{\frac{1}{2}} \theta'(0) \frac{1}{\sqrt{\sin \gamma + \cos \gamma \sigma_1}}, \quad Q_{mx} = -(Re_x)^{\frac{1}{2}} \frac{1}{\sqrt{\sigma_1 \cos \gamma + \sin \gamma}} \varphi'(0), \quad (17)$$

where $Re_x = \frac{Ux}{\nu_{hnf}}$ is the local Reynolds number with $\sigma_1 = \frac{U_\infty t}{x}$ as the non-dimensional timing parameter.

3. Entropy Generation

The equation representing the entropy generation [39,40,42,46] is

$$E'''_{gen} = \frac{k_{hnf}}{T_\infty^2} \left[\frac{\partial T}{\partial y}\right]^2 + \frac{\mu_{hnf}}{T_\infty} \left[\frac{\partial u}{\partial y}\right]^2 + \frac{RD}{C_\infty} \left[\frac{\partial C}{\partial y}\right]^2 + \frac{RD}{T_\infty} \left[\frac{\partial C}{\partial x} \frac{\partial T}{\partial x} + \frac{\partial C}{\partial y} \frac{\partial T}{\partial y}\right], \quad (18)$$

where R is the ideal gas constant while D is the diffusivity. In Equation (18), the first and second terms are respectively entropy generation due to heat transfer and viscous dissipation. The third and fourth terms are the diffusivity effects due to nanoparticles.

The characteristic entropy generation is

$$E'''_0 = \frac{k_{hnf}(T_w - T_\infty)^2}{x^2 T_\infty^2}. \quad (19)$$

The non-dimensional entropy generation rate $N_G(\zeta)$ is obtained with the help of Equation (8) as

$$N_G(\zeta) = \frac{E'''_{gen}}{E'''_0}. \quad (20)$$

So

$$N_G(\zeta) = Re(\theta')^2 + \frac{ReBr}{(\theta_w)^2}(f'')^2 + Re \frac{1}{\Phi_4} \gamma_1 \left[\frac{\varphi_w}{\theta_w}\right]^2 (\varphi')^2 + Re \frac{1}{\Phi_4} \gamma_1 \left[\frac{\varphi_w}{\theta_w}\right] \theta' \varphi', \quad (21)$$

where $Re = \frac{x^2}{\nu_{hnf} t \cos \gamma + (\nu_{hnf} x / U_\infty) \sin \gamma}$ is the Reynolds number, $\theta_w = \frac{T_w - T_\infty}{T_\infty}$ is the temperature difference parameter, $Br = \frac{\mu_{hnf} U_\infty^2}{k_{hnf} T_\infty}$ is the Brinkman number, $\gamma_1 = \frac{RDC_\infty}{k_{hnf}}$ is the diffusion constant parameter due to nanoparticles concentration and $\varphi_w = \frac{C_w - C_\infty}{C_\infty}$ is the concentration difference parameter due to nanoparticles concentration.

4. Results and Discussion

The analytical solution of Equations (9)–(14) is obtained via the homotopy analysis method (HAM) [53] and then Equation (21) is solved. All the numerical values of thermophysical properties are used from Tables 1 and 2 in computing the solution. For the influential role of parameters in flow, heat and mass transfer as well as entropy generation, $m = 0.10$, $M = 1.00$, $\lambda = 1.00$, $Sc = 1.00$, $f_w = 0.001$, $\gamma = \frac{\pi}{4}$, $Pr = 6.20$, $Re = 1.00$, $Br = 1.00$, $\gamma_1 = 1.00$, $\theta_w = 1.00$ and $\phi_w = 1.00$ are used. A comparison is made with the existing literature [19], which can be seen in Table 3. The physical sketch of the problem is shown in Figure 1. The *h*-curves are given in Figures 2–4. The parameters' effects are depicted in graphs through Figures 5–18.

Figure 5 is presented to show the influence of Lorentz forces on velocity $f'(\zeta)$. Observation from the graph reveals that velocity is decelerated for TiO$_2$/H$_2$O and GO-TiO$_2$/H$_2$O when the magnetic field parameter M increases on 1.00, 1.50 and 2.00. TiO$_2$/H$_2$O and GO-TiO$_2$/H$_2$O attain maximum velocity

near the surface. Lorentz forces decrease the flow of TiO_2/H_2O and GO-TiO_2/H_2O. Figure 6 exhibits the effect of stretching/shrinking parameter λ on velocity $f'(\zeta)$. Analysis is made for the stretching case, i.e., for $\lambda > 0$. When the surface stretches at the positive values of λ, the flow of mono nanoliquid and hybrid nanoliquid is accelerated. There is almost no distinct influential effect on velocity. Anyhow, the velocity of GO-TiO_2/H_2O is a little bit less in magnitude compared to that of TiO_2/H_2O. The reason is that the flow of TiO_2/H_2O is high due to the inclusion of one nanopaticle, while the flow of GO-TiO_2/H_2O is comparatively slow on account of two nanoparticles. Moreover, GO-TiO_2/H_2O has high viscosity compared to that of TiO_2/H_2O. The suction/injection or Stefan blowing parameter f_w effect on velocity $f'(\zeta)$ is portrayed in Figure 7. Due to suction ($f_w > 0$), near to the wall a vacant space is made. Fluid enters this vacant area to occupy it completely, consequently velocity $f'(\zeta)$ of TiO_2/H_2O and GO-TiO_2/H_2O is decreased. It is noted that in the central area of the channel, the velocity $f'(\zeta)$ is stable. Figure 8 reports that with the decreasing values of accretion/ablation parameter γ, the velocity of TiO_2/H_2O and GO-TiO_2/H_2O is also decreased. Interesting results are obtained for various values of γ. On adopting the positions $0 < \gamma < \frac{\pi}{2}$, it happens to achieve a leading edge ablation of the magnitude $U\cot\gamma$. On becoming the situation $\frac{-\pi}{4} \leq \gamma < 0$, in the backward boundary layer with trailing edge an accretion phenomenon is obtained. Implementing the case $\gamma = 0$ and $\gamma = \frac{\pi}{2}$, the system becomes similar to familiar work, such as the Blasius flat plate study and Rayleigh–Stokes study in case of hybrid nanofluid.

Figure 9 examines the influence of Prandtl number Pr on the nanoparticles temperature distribution $\theta(\zeta)$. With higher values of Pr, $\theta(\zeta)$ is diminished. Viscous forces exert a uniform effect on heat transfer for the whole of location of the channel. Figure 10 is designed to show the effect of stretching/shrinking parameter λ on temperature $\theta(\zeta)$. Both of the TiO_2/H_2O and GO-TiO_2/H_2O have shown decrement in temperature for the increasing values of λ. The temperature of the GO-TiO_2/H_2O is comparatively a little bit higher than that of TiO_2/H_2O in stretching phenomena. Figure 11 exposes that as the Stefan blowing parameter f_w increases, the temperature of TiO_2/H_2O and GO-TiO_2/H_2O is decreased. Close to the wall, the decrement in heat transfer is most prominent. Sucking extracts the heat from both of the fluids.

Figure 12 reveals that the addition in Schmidt number Sc increases the concentration. Through high values of Sc, viscosity is enhanced. Since the viscosity is the characteristic on account of cohesive forces within different layers of TiO_2/H_2O and GO-TiO_2/H_2O which have relative movement, the nanoparticles concentration $\varphi(\zeta)$ is enhanced. By dispersing the nanoparticles into the water, the viscosity enhances, resulting in an increase in the cohesive forces. Figure 13 displays the suction/injection parameter f_w, which has a dominant role in diminishing the nanoparticles concentration $\varphi(\zeta)$. Due to suction ($f_w > 0$), the nanoparticles close to the wall remained in lower numbers, so the nanoparticles concentration is dilute. Therefore, the nanoparticles concentration $\varphi(\zeta)$ decreases with increasing the suction parameter f_w.

Entropy generation rate $N_G(\zeta)$ and Reynolds number Re are projected in Figure 14. Keeping the consideration of the definition of Re, it is observed that there is an increase in entropy generation for the entire range of ζ. This is due to the addition of nanoparticles and the drag associated with them. Figure 15 is designed to show the effect on entropy generation rate by Brinkman number Br. The enhancements in Br contribute to the dynamic viscosity of TiO_2/H_2O and GO-TiO_2/H_2O. Strong cohesive forces are generated, which enhance the entropy generation rate $N_G(\zeta)$.

The Hall effect is exists on behalf of boosting the intensity of the magnetic field. Increasing the intensity of the magnetic field generates the Lorentz force resistance to the motion of mono and hybrid nanofluids (TiO_2/H_2O and GO-TiO_2/H_2O). For the clarification of the aforementioned statement, Figure 16 is drawn, where it is noticed that the flows of the fluids decrease. Flow with all its components ($f'(\zeta)$, $g(\zeta)$) reduces, which provides the deficiency of convection into the surface. Lorentz forces latent power boosts the nanoparticles volume fraction. During these conditions, the Lorentz forces work strongly on the flow, which ultimately reduces it. The irrelevance of the magnetic field for the flow for minimum value of magnetic field parameter M is likely that the enhancement of the convection through nanoparticles is

at once removed via the applicability of the magnetic field. The last term $\Phi_5 \dfrac{M(f' + mg)}{1 + m^2}$ in Equation (9) in non-dimensional form provides the proof that at low magnetic field strength and velocity $g(\zeta)$, the Hall current parameter m controls fluids motion completely. Similarly, it is evident from the last term $\Phi_5 \dfrac{M(mf' - g)}{1 + m^2}$ in Equation (10) that the velocity $g(\zeta)$ is decreased by improving the Hall current parameter m. Figure 17 authenticates that the flow component is extremely slow with the positive values of m. It may vanish completely to zero if m is enlarged.

Streamlines investigation shows the flow internal behaviors. Streamline behaviors are noticed for the Hall parameter m. The effect of this parameter shows the trapping mainly on the upper and lower portions of the surface. Figure 18 demonstrates that the trapping is same at the lower and upper portions on flow surface as the Hall parameter m assumes the value 0.60. The trapping is high to the left of the channel compared to the right portion of the surface. It is evident that the compression of streamlines are at a distance from the wall.
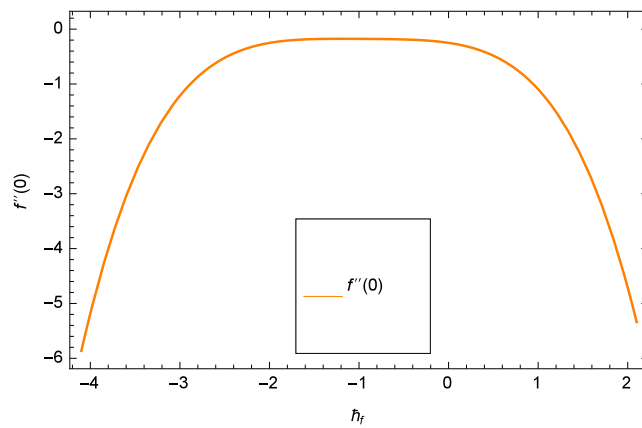
Figure 2. Representation of the $\hbar_f$ curve of $f(\zeta)$.
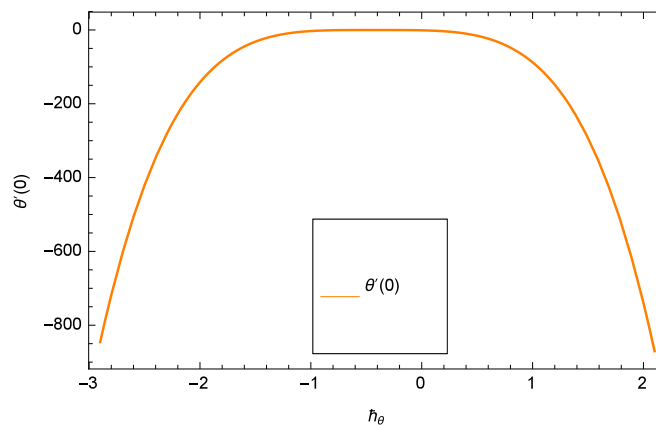
Figure 3. Representation of the $\hbar_\theta$ curve of $\theta(\zeta)$.
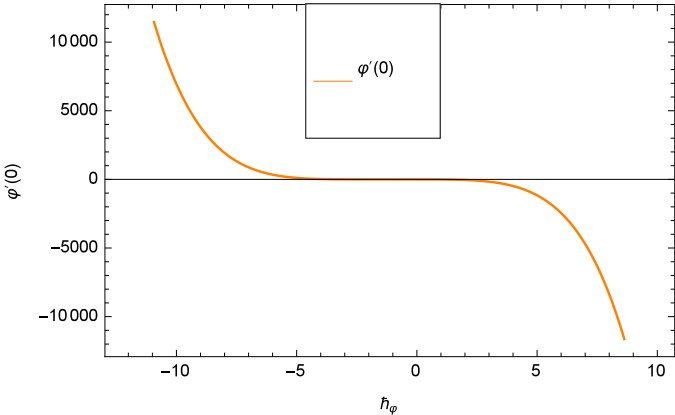
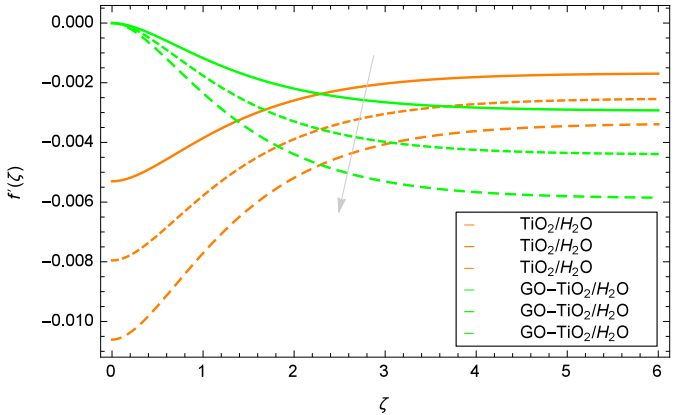**Figure 4.** Representation of the $\hbar_\varphi$ curve of $\varphi(\zeta)$.

Figure 5. Representation of the influence of a magnetic field parameter $M = 1.00, 1.50, 2.00$ on velocity $f'(\zeta)$.
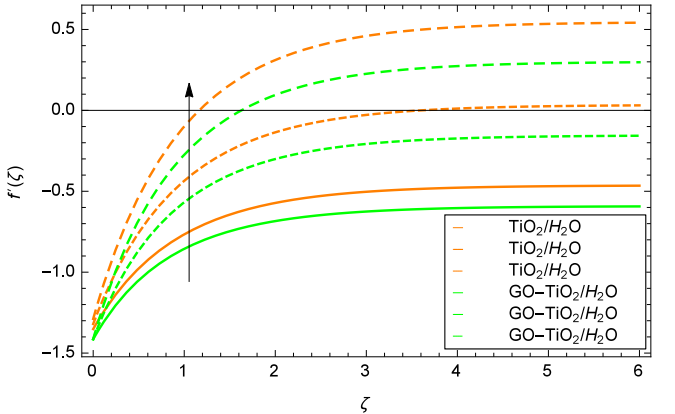

Figure 6. Representation of the influence of a stretching/shrinking $\lambda = 1.00, 1.50, 2.00$ on velocity $f'(\zeta)$.
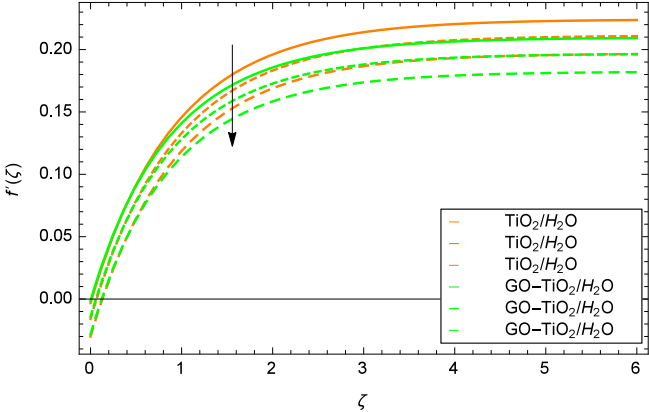
Figure 7. Representation of the influence of a Stefan blowing parameter f_w = 0.001, 0.001, 0.002 on velocity $f'(\zeta)$.
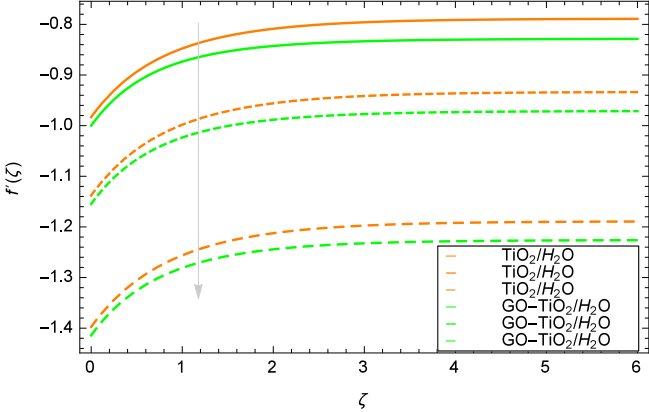

Figure 8. Representation of the influence of an accretion/ablation parameter $\gamma = \frac{\pi}{2}, \frac{\pi}{3}, \frac{\pi}{4}$ on velocity $f'(\zeta)$.
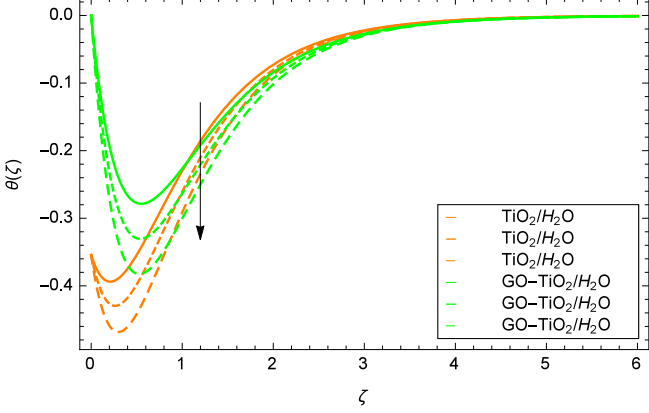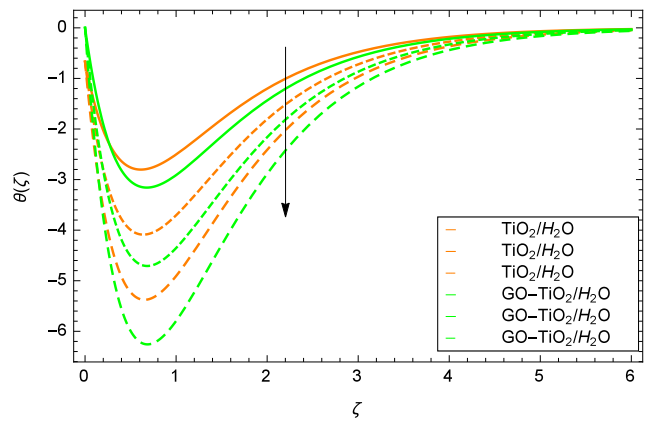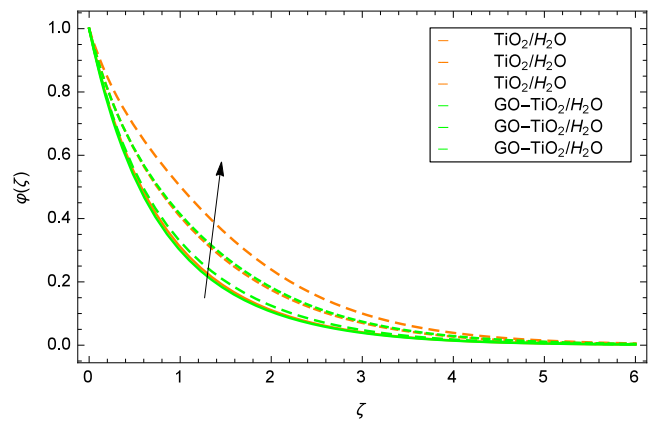

Figure 9. Representation of the influence of a Prandtl number Pr = 6.20, 8.20, 10.20 on temperature $\theta(\zeta)$.
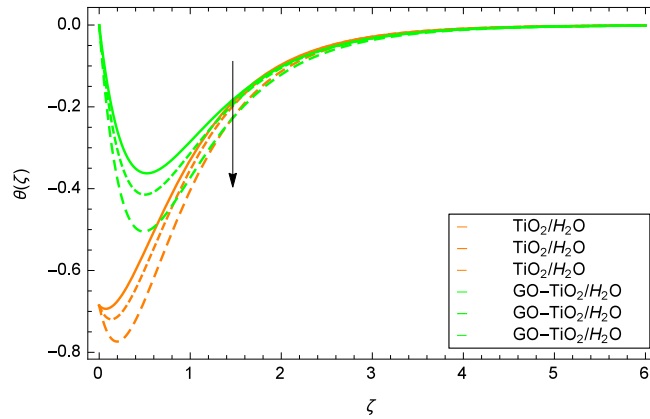
Figure 10. Representation of the influence of a stretching/shrinking parameter λ = 1.00, 1.50, 2.00 on temperature $\theta(\zeta)$.

Figure 11. Representation of the influence of a Stefan blowing parameter f_w = 1.00, 1.50, 2.00 on temperature $\theta(\zeta)$.

Figure 12. Representation of the influence of a Schmidt number Sc = 1.00, 5.00, 9.00 on nanoparticles concentration $\varphi(\zeta)$.
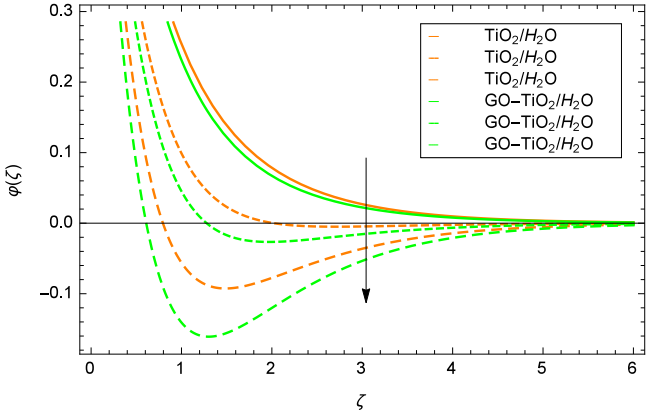
Figure 13. Representation of the influence of a Stefan blowing parameter $f_w = 1.00, 5.00, 9.00$ on nanoparticles concentration $\varphi(\zeta)$.
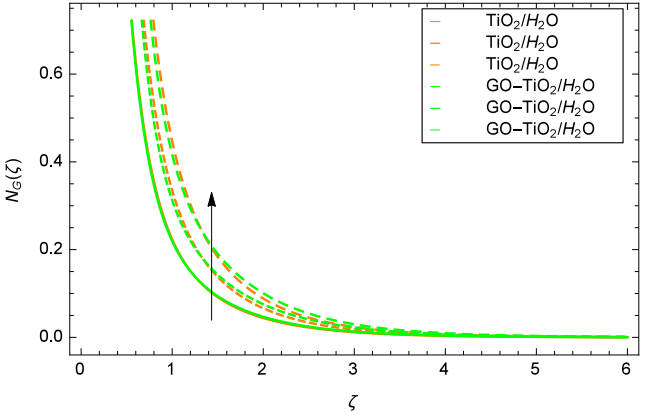
Figure 14. Representation of the influence of a Reynolds number $Re = 1.00, 1.50, 2.00$ on entropy generation rate $N_G(\zeta)$.
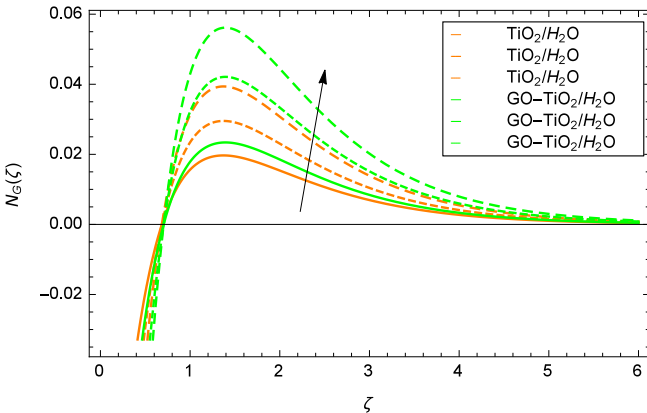
Figure 15. Representation of the influence of a Brinkman number $Br = 1.00, 1.50, 2.00$ on entropy generation rate $N_G(\zeta)$.
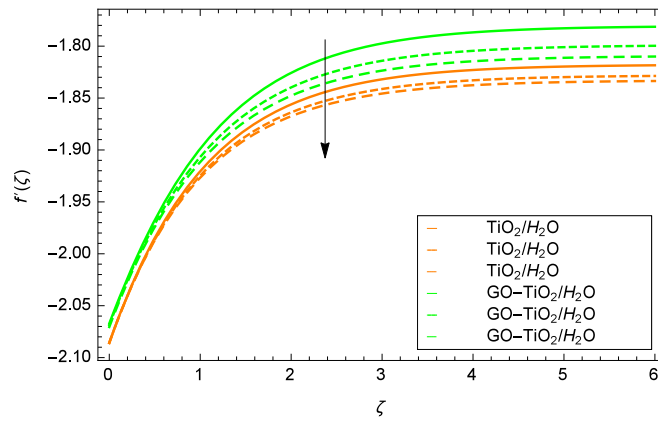
Figure 16. Representation of the influence of a Hall parameter $m = 1.00, 1.50, 2.00$ on velocity $f'(\zeta)$.
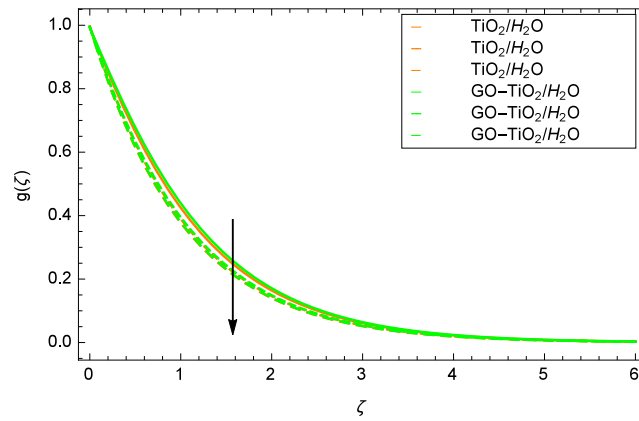

Figure 17. Representation of the influence of a Hall parameter $m = 1.00, 1.50, 2.00$ on velocity $g(\zeta)$.
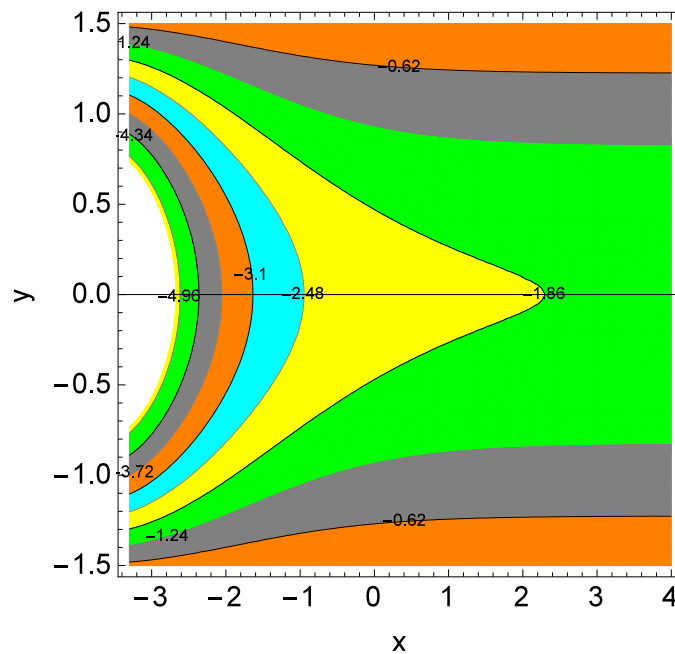

Figure 18. Representation of the influence of a Hall parameter $m = 0.60, \phi_1 = 0.03, \phi_2 = 0.04$ on streamlines.

Solution Validation

The validation of the solution is extremely important for achieving the correct results. For that purpose, the results of the present problem are compared with the study [19], although the published paper [19] has the investigations on mono nanofluid with dual solutions via bvp4c from MATLAB while the authors' study is on hybrid nanofluid, in addition to innovations like boundary conditions, entropy generation, etc. using HAM solution. But still there exists a nice agreement in computing $f''(0)$ in terms of leading edge accretion or ablation parameter γ under some conditions.

Table 3. Comparison values of $f''(0)$ in terms of parameter γ.

γ	Published Paper [19]	Present Work	Error
0^0	5.6418×10^{-1}	5.6417×10^{-1}	0.0001×10^{-1}
$(15/2)^0$	5.7501×10^{-1}	5.7500×10^{-1}	0.0001×10^{-1}
15^0	5.8072×10^{-1}	5.8071×10^{-1}	0.0001×10^{-1}
30^0	5.7700×10^{-1}	5.7700×10^{-1}	0.0000×10^{-1}
45^0	5.52287×10^{-1}	5.52285×10^{-1}	0.0002×10^{-1}
60^0	5.0721×10^{-1}	5.0720×10^{-1}	0.0001×10^{-1}
75^0	4.3686×10^{-1}	4.3684×10^{-1}	0.0002×10^{-1}
$(165/2)^0$	3.8999×10^{-1}	3.8998×10^{-1}	0.0001×10^{-1}
90^0	3.3205×10^{-1}	3.3205×10^{-1}	0.0000×10^{-1}

5. Conclusions

The nanomaterials titania and graphene oxide are used to model the heat and mass transfer flow of TiO_2/H_2O and $GO\text{-}TiO_2/H_2O$ with Hall current effect, leading edge accretion (or ablation) and entropy generation. HAM is used to generate the solution of the problem. The effects of all the parameters on different profiles are discussed in detail. The summary is presented as

(1) Velocity decreases with increasing the parameters M, f_w, γ and increases with increasing the parameter λ.
(2) Temperature decreases with increasing the parameters Pr, λ, f_w.
(3) Nanoparticles concentration decreases with increasing the parameter f_w and increases with increasing the parameter Sc.
(4) Entropy generation increases with increasing the parameters Re and Br.
(5) Both the velocity components decrease with the Hall effect parameter m.
(6) Streamlines show that the trapping increases at the left side of the surface for the parameter m.

Author Contributions: Conceptualization, N.S.K.; methodology, N.S.K.; software, P.K.; validation, Q.S. and A.B.; formal analysis, P.K.; investigation, N.S.K.; resources, P.T.; data curation, A.S.; writing—original draft preparation, N.S.K.; writing—review and editing, N.S.K.; visualization, Z.U.; supervision, N.S.K.; project administration, N.S.K.; funding acquisition, P.K. All authors have read and agreed to the published version of the manuscript.

Conflicts of Interest: The authors declare no conflict of interest.

References

1. Shatey, S.; Mosta, S. Variable viscosity on magnetohydrodynamic fluid flow and heat transfer over an unsteady stretching surface with Hall effect. *Bound. Value Probl.* **2010**, *2010*, 257568. [CrossRef]
2. Hayat, T.; Awais, M.; Nawaz, M.; Iram, S.; Alsaedi, A. Mixed convection three-dimensional flow with Hall and ion-slip effects. *Int. J. Nonlinear Sci. Numer. Simul.* **2013**, *14*, 167–177. [CrossRef]
3. Ahmed, S.; Zueco, J. Modeling of heat and mass transfer in a rotating vertical porous channel with Hall current. *Chem. Eng. Commun.* **2011**, *198*, 1294–1308. [CrossRef]
4. Gaffar, S.A.; Prasad, V.R.; Reddy, E.K. MHD free convection flow of Eyring-Powell fluid from vertical surface in porous media with Hall/ionslip currents and Ohnic dissipation. *Alex. Eng. J.* **2016**, *55*, 875–905.
5. El-Aziz, M.A. Effects of Hall current on the flow and heat transfer of a nanofluid over a stretching sheet with partial slip. *Int. J. Mod. Phys. C* **2013**, *24*, 1350044. [CrossRef]
6. Hayat, T.; Iqbal, M.; Yasmin, H.; Alsaadi, F. Hall Hall effects on peristaltic flow of couple stress fluid in an inclined asymmetric channel. *Int. J. Biomath.* **2014**, *7*, 1450057. [CrossRef]
7. Khan, N.S. Bioconvection in second grade nanofluid flow containing nanoparticles and gyrotactic microorganisms. *Braz. J. Phys.* **2018**, *43*, 227–241. [CrossRef]
8. Bahiraei, M.; Heshmatian, S. Graphene family nanofluids: A critical review and future research directions. *Energy Convers. Manag.* **2019**, *196*, 1222–1256. [CrossRef]
9. Briffa, S.M.; Lynch, I.; Hapiuk, D.; Valsami-Jones, E. Physical and chemical transformations of zirconium doped ceria nanoparticles in the presence of phosphate: Increasing realism in environmental fate and behaviour experiments. *Environ. Pollut.* **2019**, *252*, 974–981. [CrossRef]
10. Khan, N.S.; Gul, T.; Khan, M.A.; Bonyah, E.; Islam, S. Mixed convection in gravity-driven thin film non-Newtonian nanofluids flow with gyrotactic microorganisms. *Results Phys.* **2017**, *7*, 4033–4049. [CrossRef]
11. Bahiraei, M. Particle migration in nanofluids: A critical review. *Int. J. Therm. Sci.* **2016**, *109*, 90–113. [CrossRef]
12. Saba, F.; Ahmed, N.; Khan, U.; Mohyud-Din, S.T. A novel coupling of (CNT-Fe_3O_4/H_2O) hybrid nanofluid for improvements in heat transfer for flow in an asymmetric channel with dilating/squeezing walls. *Int. J. Heat Mass Transf.* **2019**, *136*, 186–195. [CrossRef]
13. Bahiraei, M.; Rahmani, R.; Yaghoobi, A.; Khodabandeh, E.; Mashayekhi, R.; Amani, M. Recent research contributions concerning use of nanofluids in heat exchangers: A critical review. *Appl. Therm. Eng.* **2018**, *133*, 137–159. [CrossRef]
14. Waini, I.; Ishak, A.; Pop, I. Unsteady flow and heat transfer past a stretching/shrinking sheet in a hybrid nanofluid. *Int. J. Heat Mass Transf.* **2019**, *136*, 288–297. [CrossRef]
15. Bahiraei, M.; Heshmatian, S. Electronic cooling with nanofluids: A critical review. *Energy Convers. Manag.* **2018**, *172*, 438–456. [CrossRef]
16. Gulzar, O.; Qayoum, A.; Gupta, R. Experimental study on stability and rheological behaviour of hybrid Al_2O_3-TiO_2 Therminol-55 nanofluids for considering solar collectors. *Powder Technol.* **2019**, *352*, 436–444. [CrossRef]
17. Dalkilic, A.S.; Turk, O.A.; Mercan, H.; Nakkaew, S. An experimental investigation on heat transfer characteristics of graphite-SiO_2/water hybrid nanofluid flow in horizontal tube with various quad-channel twisted tape inserts. *Int. Commun. Heat Mass Transf.* **2019**, *107*, 1–13. [CrossRef]
18. Khan, N.S.; Gul, T.; Islam, S.; Khan, I.; Alqahtani, A.M.; Alshomrani, A.S. Magnetohydrodynamic nanoliquid thin film sprayed on a stretching cylinder with heat transfer. *J. Appl. Sci.* **2017**, *7*, 271. [CrossRef]
19. Rosca, N.C.; Pop, I. Unsteady boundary layer flow of a nanofluid past a moving surface in an external uniform free stream using Buongiorno's model. *Comput. Fluids* **2014**, *95*, 49–55. [CrossRef]
20. Zuhra, S.; Khan, N.S.; Khan, M.A.; Islam, S.; Khan, W.; Bonyah, E. Flow and heat transfer in water based liquid film fluids dispensed with graphene nanoparticles. *Results Phys.* **2018**, *8*, 1143–1157. [CrossRef]
21. Khan, N.S.; Gul, T.; Islam, S.; Khan, W. Thermophoresis and thermal radiation with heat and mass transfer in a magnetohydrodynamic thin film second-grade fluid of variable properties past a stretching sheet. *Eur. Phys. J. Plus* **2017**, *132*, 11. [CrossRef]

22. Palwasha, Z.; Khan, N.S.; Shah, Z.; Islam, S.; Bonyah, E. Study of two dimensional boundary layer thin film fluid flow with variable thermo-physical properties in three dimensions space. *AIP Adv.* **2018**, *8*, 105318. [CrossRef]

23. Khan, N.S.; Gul, T.; Islam, S.; Khan, A.; Shah, Z. Brownian motion and thermophoresis effects on MHD mixed convective thin film second-grade nanofluid flow with Hall effect and heat transfer past a stretching sheet. *J. Nanofluids* **2017**, *6*, 812–829. [CrossRef]

24. Khan, N.S.; Zuhra, S.; Shah, Z.; Bonyah, E.; Khan, W.; Islam, S. Slip flow of Eyring-Powell nanoliquid film containing graphene nanoparticles. *AIP Adv.* **2019**, *8*, 115302. [CrossRef]

25. Khan, N.S.; Gul, T.; Kumam, P.; Shah, Z.; Islam, S.; Khan, W.; Zuhra, S.; Sohail, A. Influence of inclined magnetic field on Carreau nanoliquid thin film flow and heat transfer with graphene nanoparticles. *Energies* **2019**, *12*, 1459. [CrossRef]

26. Khan, N.S. Study of two dimensional boundary layer flow of a thin film second grade fluid with variable thermo-physical properties in three dimensions space. *Filomat* **2019**, *33*, 5387–5405. [CrossRef]

27. Khan, N.S.; Zuhra, S. Boundary layer unsteady flow and heat transfer in a second grade thin film nanoliquid embedded with graphene nanoparticles past a stretching sheet. *Adv. Mech. Eng.* **2019**, *11*, 1–11. [CrossRef]

28. Khan, N.S.; Gul, T.; Islam, S.; Khan, W.; Khan, I.; Ali, L. Thin film flow of a second-grade fluid in a porous medium past a stretching sheet with heat transfer. *Alex. Eng. J.* **2017**, *57*, 1019–1031. [CrossRef]

29. Zuhra, S.; Khan, N.S.; Alam, A.; Islam, S.; Khan, A. Buoyancy effects on nanoliquids film flow through a porous medium with gyrotactic microorganisms and cubic autocatalysis chemical reaction. *Adv. Mech. Eng.* **2020**, *12*, 1–17. [CrossRef]

30. Palwasha, Z.; Islam, S.; Khan, N.S.; Ayaz, H. Non-Newtonian nanoliquids thin film flow through a porous medium with magnetotactic microorganisms. *Appl. Nanosci.* **2018**, *8*, 1523–1544. [CrossRef]

31. Khan, N.S. Mixed convection in MHD second grade nanofluid flow through a porous medium containing nanoparticles and gyrotactic microorganisms with chemical reaction. *Filomat* **2019**, *33*, 4627–4653. [CrossRef]

32. Zuhra, S.; Khan, N.S.; Shah, Z.; Islam, Z.; Bonyah, E. Simulation of bioconvection in the suspension of second grade nanofluid containing nanoparticles and gyrotactic microorganisms. *AIP Adv.* **2018**, *8*, 105210. [CrossRef]

33. Khan, N.S.; Shah, Z.; Shutaywi, M.; Kumam, P.; Thounthong, P. A comprehensive study to the assessment of Arrhenius activation energy and binary chemical reaction in swirling flow. *Sci. Rep.* **2020**, *10*, 7868. [CrossRef] [PubMed]

34. Zuhra, S.; Khan, N.S.; Islam, S. Magnetohydrodynamic second grade nanofluid flow containing nanoparticles and gyrotactic microorganisms. *Comput. Appl. Math.* **2018**, *37*, 6332–6358. [CrossRef]

35. Zuhra, S.; Khan, N.S.; Islam, S.; Nawaz, R. Complexiton solutions for complex KdV equation by optimal homotopy asymptotic method. *Filomat* **2020**, *33*, 6195–6211. [CrossRef]

36. Zahra, A.; Mahanthesh, B.; Basir, M.F.M.; Imtiaz, M.; Mackolil, J.; Khan, N.S.; Nabwey, H.A.; Tlili, I. Mixed radiated magneto Casson fluid flow with Arrhenius activation energy and Newtonian heating effects: Flow and sensitivity analysis. *Alex. Eng. J.* **2020**, *57*, 1019–1031.

37. Liaqat, A.; Asifa, T.; Ali, R.; Islam, S.; Gul, T.; Kumam, P.; Mukhtar, S.; Khan, N.S.; Thounthong, P. A new analytical approach for the research of thin-film flow of magneto hydrodynamic fluid in the presence of thermal conductivity and variable viscosity. *ZAMM J. Appl. Math. Mech. Z. Angewwandte Math. Mech.* **2020**, 1–13. [CrossRef]

38. Bejan, A. Second law analysis in heat transfer. *Energy* **1980**, *5*, 720–732. [CrossRef]

39. Ahmad, S.; Nadeem, S. Flow analysis by Cattaneo-Christov heat flux in the presence of Thomson and Troian slip condition. *Appl. Nanosci.* **2020**. [CrossRef]

40. Khan, N.; Riaz, I.; Hashmi, M.S.; Musmar, S.A.; Khan, S.U.; Abdelmalek, Z.; Tlili, I. Aspects of chemical entropy generation in flow of Casson nanofluid between radiative stretching disks. *Entropy* **2020**, *22*, 495. [CrossRef]

41. Khan, N.S.; Zuhra, S.; Shah, Q. Entropy generation in two phase model for simulating flow and heat transfer of carbon nanotubes between rotating stretchable disks with cubic autocatalysis chemical reaction. *Appl. Nanosci.* **2019**, *9*, 1797–1822. [CrossRef]

42. Zaib, A.; Khan, U.; Shah, Z.; Kumam, P.; Thounthong, P. Optimization of entropy generation in flow of micrpolar mixed convective magnetite (Fe_3O_4) ferroparticle over a vertical plate. *Alex. Eng. J.* **2019**, *58*, 1461–1470.

43. Khan, N.S.; Shah, Z.; Islam, S.; Khan, I.; Alkanhal, T.A.; Tlili, I. Entropy generation in MHD mixed convection non-Newtonian second-grade nanoliquid thin film flow through a porous medium with chemical reaction and stratification. *Entropy* **2019**, *21*, 139. [CrossRef]

44. Shahsavar, A.; Baseri, M.M.; Al-Rashed, A.A.A.A.; Afrand, M. Numerical investigation of forced convection heat transfer and flow irreversibility in a novel heat sink with helical microchannels working with biologically synthesized water-silver nano-fluid. *Int. Commun. Heat Mass Transf.* **2019**, *108*, 104324. [CrossRef]

45. Khan, N.S.; Zuhra, S.; Shah, Z.; Bonyah, E.; Khan, W.; Islam, S.; Khan, A. Hall current and thermophoresis effects on magnetohydrodynamic mixed convective heat and mass transfer thin film flow. *J. Phys. Commun.* **2019**, *3*, 035009. [CrossRef]

46. Sohail, M.; Naz, R.; Abdelsalam, S.I. On the onset of entropy generation for a nanofluid with thermal radiation and gyrotactic microorganisms through 3D flows. *Phys. Scr.* **2019**, *95*, 045206. [CrossRef]

47. Shah, Z.; Kumam, P.; Deebani, W. Radiative MHD Casson nanofluid flow with activation energy and chemical reaction over nonlinear stretching surface through entropy generation. *Sci. Rep.* **2020**, *10*, 4402. [CrossRef]

48. Khan, N.S.; Kumam, P.; Thounthong, P. Renewable energy technology for the sustainable development of thermal system with entropy measures. *Int. J. Heat Mass Transf.* **2019**, *145*, 118713. [CrossRef]

49. Khan, N.S.; Kumam, P.; Thounthong, P. Second law analysis with effects of Arrhenius activation energy and binary chemical reaction on nanofluid flow. *Sci. Rep.* **2020**, *10*, 1226. [CrossRef]

50. Khan, N.S.; Shah, Q.; Bhaumik, A.; Kumam, P.; Thounthong, P.; Amiri, I. Entropy generation in bioconvection nanofluid flow between two stretchable rotating disks. *Sci. Rep.* **2020**, *10*, 4448. [CrossRef]

51. Khan, N.S.; Shah, Q.; Sohail, A. Dynamics with Cattaneo-Christov heat and mass flux theory of bioconvection Oldroyd-B nanofluid. *Adv. Mech. Eng.* **2020**. [CrossRef]

52. Rahila, N.; Noor, M.; Shah, Z.; Sohail, M.; Kumam, P.; Thounthong, P. Entropy generation optimization in MHD pseudoplastic fluid comprising motile microorganisms with stratification effect. *Alex. Eng. J.* **2020**, *59*, 485–496.

53. Liao, S.J. *Homotopy Analysis Method in Nonlinear Differential Equations*; Higher Education Press: Beijing, China; Springer: Berlin/Heidelberg, Germany, 2012.